ARTICLES

Recognition Mechanism of Theophylline-Imprinted Polymers: Two-Dimensional Infrared Analysis and Density Functional Theory Study

Ai-Fu Che, Ling-Shu Wan, Jun Ling, Zhen-Mei Liu, and Zhi-Kang Xu*

Key Laboratory of Macromolecular Synthesis and Functionalization (Ministry of Education), Department of Polymer Science and Engineering, Zhejiang University, Hangzhou 310027, P.R. China

Received: August 4, 2008; Revised Manuscript Received: April 2, 2009

Molecular imprinting polymers (MIPs) are synthetic materials having specific cavities tailored for a target molecule. Thoroughly understanding the molecular recognition mechanism is favorable for the rational design, preparation, and application of MIPs. In this work, theophylline (THO)-imprinted poly(acrylonitrile-*co*-acrylic acid) (PANCAA) films with acrylic acid (AA) as the functional monomer were fabricated and a set of concentration-dependent Fourier transform infrared (FT-IR) spectra were collected. Two-dimensional (2D) correlation analysis of the spectra and density functional theory (DFT) calculation were conducted to evaluate the molecular recognition mechanism. DFT at the B3LYP/6-31+G(d,p) level is efficacious to calculate the binding energies (ΔE) and the theoretical vibration frequencies for the possible configurations of THO_AA complexes. An optimized cyclic hydrogen-bonded configuration (complex THO_AA1) has the highest binding energy (-16.63 kcal mol^{-1}) that is more stable than others. In addition, the experimental vibrations of the carbonyl groups in the FT-IR spectra were assigned on the basis of the DFT results. Moreover, methylacrylic acid (MAA) and caffeine (CAF) as compared analogues were also investigated. The DFT-based theoretical predictions are coincident with the reported results.

Introduction

Molecular imprinting polymers (MIPs) are synthetic materials with specific recognition sites complementary in shape, size, and functional groups to the template molecule. These recognition sites can mimic the binding sites of biological entities such as antibodies and enzymes. Over the past 30 years, two distinct imprinting approaches have been employed for the preparation of MIPs. In the covalent approach pioneered by Wulff and co-workers,[1] the "template−monomer" complex is formed through the reversible chemical bonds between the template and the functional monomers. In the noncovalent approach that was first reported by Mosbach and co-workers,[2] the template−monomer complex is formed through the noncovalent interactions such as hydrogen bonds, van der Waals forces, ionic interactions and hydrophobic effects. Because of the stability, easy of preparation, low cost and high selectivity for most of target analytes, various MIPs for chiral recognition,[3,4] membrane separation,[5] solid phase extraction,[6,7] catalysis,[8] drug assay,[9] and sensing[10,11] have been extensively reported.

A MIP is usually synthesized for a specific analytical use that implies the choice of a given template molecule. Among various templates, theophylline (THO) is one kind of xanthine derivative with a variety of medical applications. THO-imprinted polymers in the forms of microspheres[12] and membranes[13−16] have been already successfully prepared since the first report in 1993.[17] Experimental results indicate that the THO-imprinted polymers can rebind the template molecule obviously and have a high selectivity to THO in comparison to its structural analogues such as caffeine (CAF) and theobromine (THB). Several techniques including nuclear magnetic resonance (^{1}H NMR),[2,18,19] Fourier transform infrared (FT-IR) spectroscopy,[20,21] and ultraviolet (UV) spectroscopy[22,23] were applied to study the molecular recognition mechanism of MIPs. In consequence, hydrogen bonds between the THO molecule and the functional groups were considered as the dominant driving force in these cases.[13,24,25] With the development of computational chemistry, mathematical simulation has been considered as a simple and fast approach to study the recognition mechanism in the imprinting process at a molecular level. In this context, recent work is mainly focused on two aspects for the THO-imprinted polymers. One is to screening functional monomers for the rational design of MIPs. Molecular dynamics simulations were first carried out to select suitable monomers/polymers for THO by Pavel et al.[26,27] Subsequently, a more reliable DFT method (B3LYP/6-31+G**) was employed to screen monomers for the synthesis of THO-imprinted polymers using binding energy as a measure in Liu's group.[25] This process is time-saving, efficient, and predictable for the preparation of THO-imprinted polymers. The other is to clarify the imprinting mechanism. Quantum mechanical calculations at RHF/6-31G* level were applied to study the interactions between the THO molecule and the functional monomers.[26] However, it seems that the DFT method is a more suitable approach due to its high accuracy and reliability.[28] In addition, two-dimensional (2D) correlation spectroscopy proposed by Noda[29,30] may be a superior technique to analyze the molecular interactions, which can provide useful information unavailable in one-dimensional (1D) spectroscopy. For example, 2D correlation spectra were effective for uncover-

* Corresponding author. E-mail: xuzk@zju.edu.cn. Fax: +86 571 8795 1773.

10.1021/jp902163s CCC: $40.75
Published on Web 04/29/2009

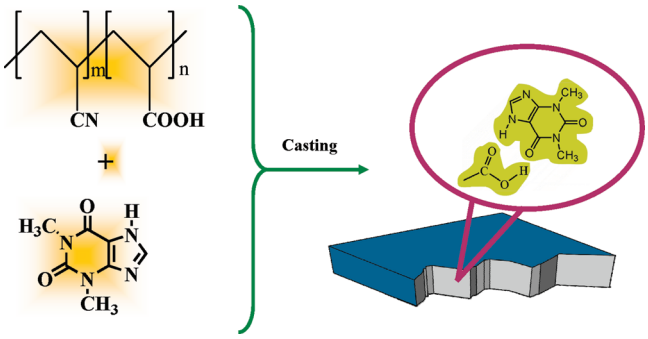

Figure 1. Schematic representation of THO-imprinted PANCAA film.

ing the overlapped bands and identifying the sequence of band intensity changes.[31,32]

To our knowledge, the 2D correlation analysis of Fourier transform infrared (2D IR) spectroscopy has not yet been applied for the molecular imprinting process. Therefore, 2D FT-IR and DFT-based theoretical prediction was used to further elucidate the molecular interactions between the THO template and the functional groups in the MIPs. It can be certainly envisaged that this work will be favorable for understanding the molecular recognition mechanism of MIPs. For this purpose, THO-imprinted films were prepared from poly(acrylonitrile-*co*-acrylic acid) (PANCAA) with AA as the functional monomer and THO as the template (Figure 1). A set of concentration-dependent FT-IR spectra were acquired and analyzed by 2D correlation technique. To fulfill the assignment of experimental frequencies of the THO-imprinted films, the DFT method (B3LYP/6-31+G**) was used to calculate the binding energies and the theoretical frequencies of the possible configurations THO_AA complexes.

Experimental Section

Materials. Acrylonitrile (AN), AA, and dimethyl sulfoxide (DMSO) were commercially obtained from Shanghai Chemical Agent Co. and distilled under reduced pressure before use. Azoisobutyronitrile (AIBN) was recrystallized in ethanol at 40 °C. THO was purchased from Sigma and used as received. PANCAA (M_η = 2.4 × 10^5 g/mol) was synthesized in our laboratory.[33] The AA content in PANCAA is 15.3 mol %.

Film Preparation. THO-imprinted films ([THO]/[COOH] = 1/8, 1/4, 3/8, 5/8, respectively) and PANCAA film were prepared by casting the corresponding solutions on clean glass plates. The solvent was evaporated under reduced pressure at 40 °C for 24 h and further dried at 80 °C for 24 h. Then, the films were peeled off and put in a vacuum oven at 80 °C for another 24 h and finally cooled slowly down to room temperature. The thickness of the films were approximately 20 ± 2 μm measured by a screw micrometer.

Transmission FT-IR. Infrared spectra were taken by 32 scans at a nominal resolution of 1 cm^{-1} using a FT-IR spectrometer (Nicolet, Nexus-470). All the spectra were baseline-corrected and normalized to the same thickness on the basis of the 2242 cm^{-1} band of the acrylonitrile segment.

2D IR Correlation Analysis. 2D correlation analysis using a software program (2Dshige (c) Shigeaki Morita, Kwansei-Gakuin University, 2004−2005) was conducted for the concentration-dependent FT-IR spectra of the THO-imprinted films. In the 2D correlation maps, the unshaded regions indicate positive correlation intensities, whereas the shaded ones are negative.

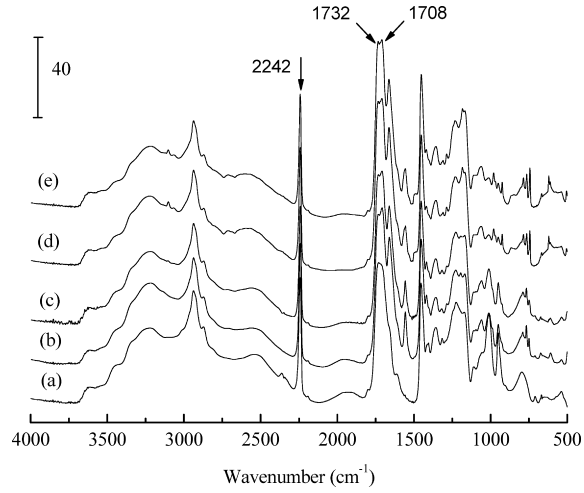

Figure 2. FT-IR spectra of (a) PANCAA film and THO-imprinted films with molar ratios of [THO]/[COOH] at (b) 1/8, (c) 1/4, (d) 3/8, and (e) 5/8.

Computational Methods. To provide detailed assignments for the transmission FT-IR spectra and the 2D IR correlation spectra, the DFT method, which is relatively reliable and accurate for calculations,[28,34] was employed to calculate the binding energies and the theoretical frequencies. The geometry optimizations followed by frequency calculations of the model compounds were carried out using hybrid density functional Becke3−Lee−Yang−Parr (B3LYP) with a 6-31+G(d,p) basis set (B3LYP/6-31+G(d,p)).[35] All the calculations were performed using Gaussian 03 program package.[36]

The conformation optimization and energy calculation was also applied to the template-monomer complex. The binding energy was calculated from the equation below:

$$\Delta E = E_{\text{complex}} - (E_{\text{template}} + E_{\text{monomer}})$$

where E_{complex}, E_{template}, and E_{monomer} are energies of the complex, the template, and the monomer, respectively. The zero-point vibrational energy (ZPVE) correction is scaled by a factor of 0.975.

In the theoretical calculations, a methyl-ended acrylic acid unit was used. The best agreement between the calculated and the observed frequencies occurs when the calculated frequencies are scaled by 0.975.[37]

Results and Discussion

FT-IR Spectra. Figure 2 shows a set of concentration-dependent FT-IR spectra for the THO-imprinted PANCAA films in the region 4000 to 400 cm^{-1}. In the C═O stretching region, the intensity of the broad band increases with the THO concentration. In addition, the striking band centered at 1732 cm^{-1} shows a significant low frequency shift to that at 1708 cm^{-1}. The shift is probably because of the strong interactions between the THO molecule and the carboxyl groups of PANCAA. To get an insight into the interactions between the template molecule and the functional groups, the overlapped bands should be resolved and assigned definitely. Recently, 2D IR correlation analysis has been proved to be a powerful tool that is capable of separating and identifying highly overlapped bands.[29,30]

2D IR Correlation Analysis. Generalized 2D IR correlation spectroscopy,[38] which is an extension of the original 2D IR correlation spectroscopy,[29,30] is generated from a set of sequential 1D IR spectra under the external perturbation that is not only

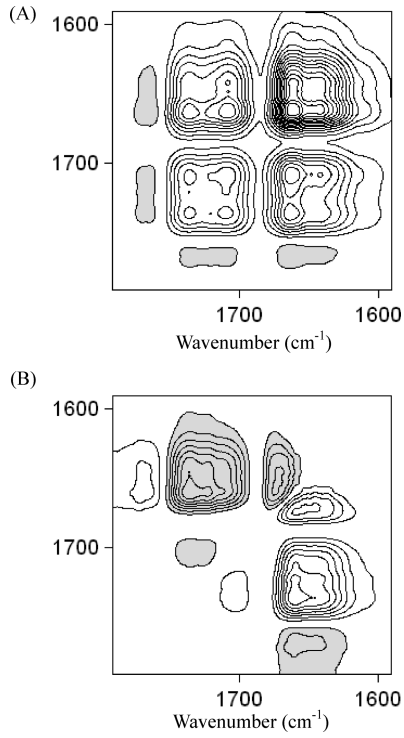

Figure 3. (A) Synchronous and (B) asynchronous 2D correlation contour maps of concentration-dependent FT-IR spectra at the spectral range between 1800 and 1600 cm^{-1}. Shaded area indicates negative correlation.

TABLE 1: Calculated Binding Energies (ΔE) of THO with AA Unit and MAA Unit

molecules	energy (hartree)	ΔE (Hartree)	ΔE (kcal mol^{-1})
THO	−641.1002229		
AA	−347.057464		
MAA	−386.3719095		
complex THO_AA1	−988.1860195	−0.0265	−16.63
complex THO_AA2	−988.1710162	−0.01174	−7.36
complex THO_AA3	−988.1744635	−0.01503	−9.43
complex THO_AA4	−988.1742251	−0.01511	−9.48
complex THO_MAA1	−1027.5004851	−0.02655	−16.66

the time but also any other physical variables such as temperature,[39,40] concentration,[41] and composition.[42,43] In our work, the THO concentration was used as the external perturbation. As shown in Figure 3, 2D IR correlation spectra in the 1800−1600 cm^{-1} region are constructed by the concentration-dependent FT-IR spectra. The synchronous and asynchronous spectra provide different information, according to the rules proposed by Noda.[38] In synchronous spectrum ($\Phi(\nu_1/\nu_2)$), the synchronous peaks represent the relative similarity of the intensity variation behavior. The sign of peaks becomes positive if the two intensity variations occur simultaneously in the same direction (either increasing or decreasing), whereas the negative sign of peaks indicates that one of the spectral intensity is increasing and the other is decreasing. In Figure 3A, the broad band in the C═O stretching region splits into four distinct peaks located at diagonal positions that are 1735, 1708, 1661, and 1642 cm^{-1}. The obvious positive cross peaks (1735/1708, 1735/1661, 1735/1642, 1661/1642 cm^{-1}) indicate in-phase intensity

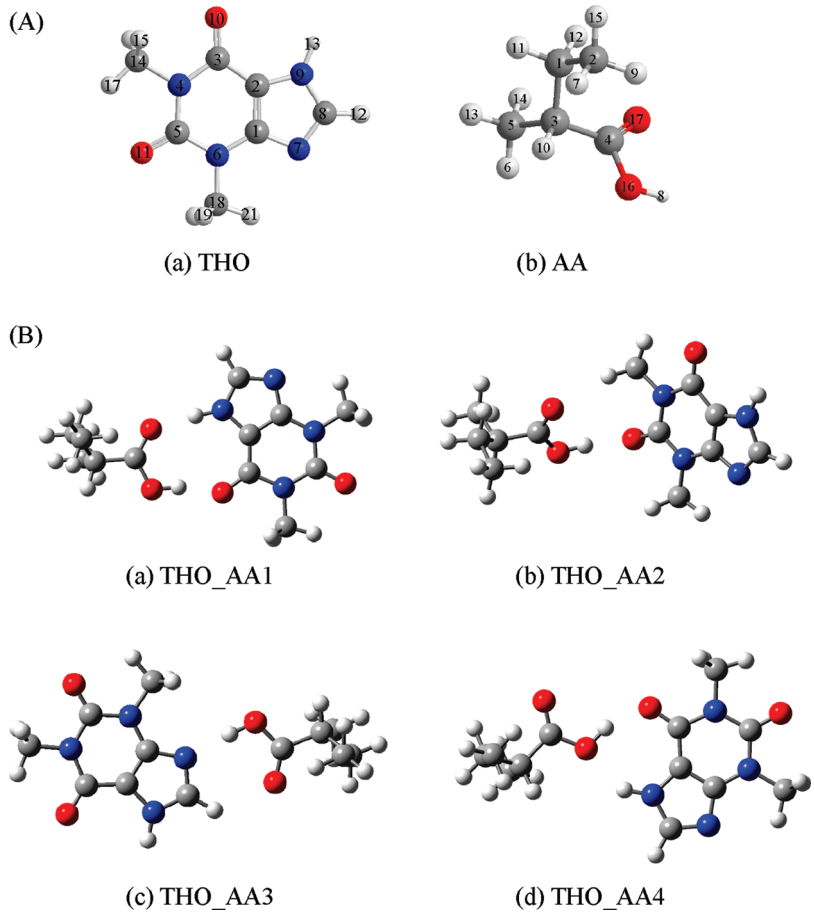

Figure 4. Optimized structures of (A) THO and methyl-ended AA unit labeled with serial numbers and (B) four possible optimized configurations for complexes of THO_AA.

TABLE 2: Calculated Results by DFT Analysis and Assignments of Bands in FT-IR and 2D Correlation Spectra

calculated wavenumber[a]	measured 1D FT-IR wavenumber	measured 2D-IR wavenumber	assignments (C═O stretching vibrations)
1764		1767	free COOH groups
1734	1732	1735	AA unit in the complex of THO_AA2
1722		1723	AA unit in the complex of THO_AA3
1691	1709	1708	AA unit in the complex of THO_AA1
		1673	oligomeric COOH groups
1657	1663	1661	THO in the complex THO_THO
1645		1646	THO in the complex of THO_AA1

[a] Calculated frequencies are scaled by a factor of 0.975.

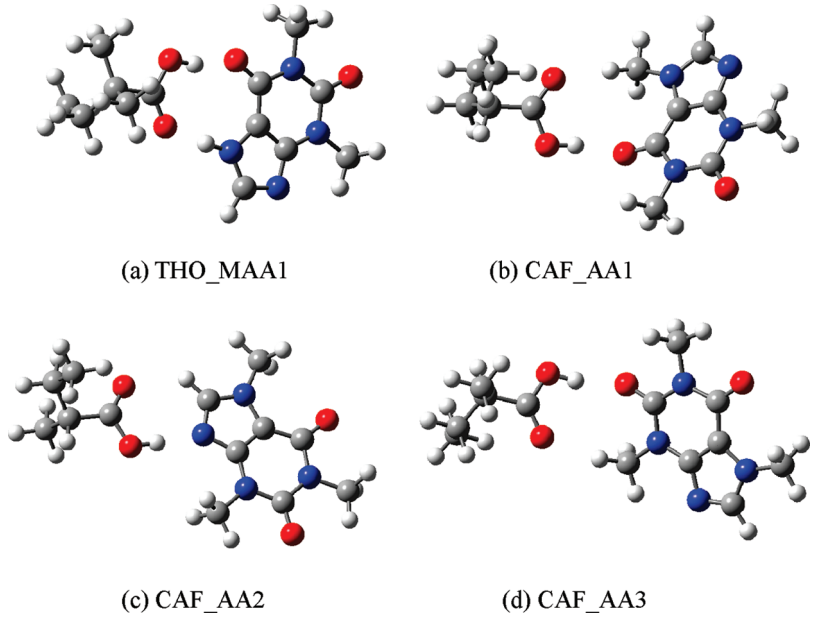

Figure 5. Optimized configurations for complexes of THO_MAA and CAF_AA.

TABLE 3: Calculated Binding Energies (ΔE) of CAF with AA Unit

molecules	energy (hartree)[a]	ΔE (Hartree)	ΔE (kcal mol^{-1})
CAF	−680.4140895		
AA	−347.057464		
complex CAF_AA1	−1027.4867331	−0.01356	−8.51
complex CAF_AA2	−1027.4882234	−0.01537	−9.64
complex CAF_AA3	−1027.4856241	−0.01249	−7.84

[a] ZPVE correction is scaled by a factor of 0.975.

variations. The negative cross peaks (1767/1735, 1767/1708, 1767/1661, 1767/1642 cm^{-1}) suggest that the C═O stretching vibration at 1767 cm^{-1} and others are changing in the opposite direction. In the asynchronous spectrum ($\Psi(\nu_1/\nu_2)$), the asynchronous cross peaks imply the relative dissimilarity of the intensity variation behavior, which can uncover the highly overlapped bands. Furthermore, the sign of cross peaks in the asynchronous spectrum provides information about the sequence of the intensity variations with a high level of certainty. According to the Noda's rule, in the region of $\nu_1 > \nu_2$, the sign of the cross peaks becomes positive if the intensity variation at ν_1 occurs predominantly before that at ν_2 with the increase of THO concentration, whereas it becomes negative if the intensity variation occurs after that at ν_2.[41−43] The relationship is reverse in the region of $\nu_1 < \nu_2$. As can be seen from Figure 3B, the highly overlapped band can be further separated into 1767, 1735, 1723, 1708, 1673, 1661, and 1645 cm^{-1}. The strong cross peaks (1767/1661, 1735/1661, 1723/1661, 1708/1661, 1673/1661 cm^{-1}) indicate that the band at 1661 cm^{-1} shows asynchronicity with those at 1767, 1735, 1723 1708 and 1673 cm^{-1}. Similar results are obtained from the cross peaks (1767/1645, 1735/1645, 1723/1645, 1708/1645 and 1673/1645 cm^{-1}). As reported in the relevant literature,[44,45] the bands at 1767, 1735, 1723, 1708, and 1673 cm^{-1} can be assigned to C═O stretching vibrations of COOH groups. Therefore, the bands at 1661 and 1645 cm^{-1} may be ascribed to C═O stretching vibrations of THO. In addition, the positive cross peaks (1767/1661 and 1767/1645 cm^{-1}) suggest that the band at 1767 cm^{-1} varies at a lower THO concentration compared to those at 1661 and 1645 cm^{-1}. While the evident negative cross peaks indicate those bands (1735, 1723, 1708, and 1673 cm^{-1}) occur at a higher THO concentration than those at 1661 and 1645 cm^{-1}. The sequential order of intensity changes has provided additional information in comparison with 1D IR spectra. However, what are the possible assignments of these separated bands?

DFT Analysis and Assignments of the 2D IR Correlation Spectra. Theoretical calculations were carried out to assist in assigning the characteristic peaks and further elucidate the interactions between THO and the functional groups. To simplify the structure of PANCAA, a methyl-ended AA unit was employed as the model compound for calculation. The energies of model molecules (Figure 4A) with optimized conformation were calculated. The Mulliken charges of the atoms in THO and the functional unit were obtained, as previously reported.[25] For THO, H_{13} is the proton donor, N_7, O_{10}, and O_{11} are the proton acceptors, while for the AA unit, H_8 is the proton donor and O_{16} and O_{17} are the proton acceptors.

TABLE 4: Binding Capacity and Selectivity of Different THO-Imprinted Polymers

polymers[a]	COOH (mol %)	THO	CAF	reference
P(MMA-*co*-AA) membrane entrapped with THO-imprinted P(MMA-*co*-AA) particles	10	5.3 μM/g membrane		16
P(MMA-*co*-AA) membrane entrapped with CAF-imprinted P(MMA-*co*-AA) particles	10		0.55 μM/g membrane	16
magnetic THO-imprinted polymer nanowires		11.8 $\pm$ 1.1 μM/g polymer	2.4 $\pm$ 0.3 μM/g polymer	19
THO-imprinted P(AN-*co*-AA) membrane	14.4	1.35 μM/g polymer	0.22 μM/g polymer	13
THO-imprinted P(AN-*co*-MAA) membrane	13.3	1.22 μM/g polymer	0.33 μM/g polymer	13
THO-imprinted PMAA microsphere		57 $\pm$ 12 nm/g polymer		51
P(MMA-*co*-AA) membrane entrapped with THO-imprinted P(MMA-*co*-MAA) nanoparticle	75	0.95 mg/g polymer	0.095 mg/g polymer	52
P(MMA-*co*-AA) membrane deposited by CAF-imprinted P(MMA-*co*-MAA) nanoparticle	75	0.109 mg/g polymer	0.029 mg/g polymer	52
THO-imprinted PAA layer on PAN membrane surface		8.8 μM/m^2 membrane	1.5 μM/m^2 membrane	53
THO-imprinted PMAA layer on cellulose surface		3.26 $\pm$ 0.18 μm/s	2.91 $\pm$ 0.25 μm/s	54

[a] P(MMA-*co*-AA), poly(methyl methacrylate-*co*-acrylic acid); P(AN-*co*-AA), poly(acrylonitrile-*co*-acrylic acid); P(AN-*co*-MAA): poly(acrylonitrile-*co*-methylacrylic acid); PMAA, poly(methylacrylic acid); P(MMA-*co*-MAA), poly(methyl methacrylate-*co*-methylacrylic acid); PAA, poly(acrylic acid).

According to the hydrogen bond formation principle and the geometry, four possible configurations of the complexes were constructed and optimized (Figure 4). The corresponding binding energies (ΔE) are summarized in Table 1. It is found that configuration 1 (Figure 4B) has the highest binding energy (-16.63 kcal·mol^{-1}) and the value is nearly twice as much as other configurations, which indicates that this kind of cyclic hydrogen-bonded structure will be a more stable form.

Based on the optimized structures, calculated frequencies were obtained accordingly, which can assist the assignment of experimental vibrational frequencies.[46−48] The calculation results show that the band at 1767 cm^{-1} is attributed to the C═O stretching vibration of free COOH groups. The bands at 1735 and 1723 cm^{-1} are derived from C═O stretching vibrations of the residual carbonyl groups in the complex THO_AA2 and complex THO_AA3, respectively. Moreover, the band at 1673 cm^{-1} may be assigned to C═O stretching vibration of the oligomeric COOH groups, as reported the literature.[45] Strikingly, the bands at 1708 and 1646 cm^{-1} can be ascribed to C═O stretching vibrations of AA and THO in the stable cyclic structure between THO and the functional groups according to the calculated frequencies of the complex THO_AA1 (1691 and 1645 cm^{-1}). In addition, on the basis of the calculated frequency of complex THO_THO (1657 cm^{-1}), the evident band at 1661 cm^{-1} in the 2D IR spectra may be ascribed to the C═O stretching vibration of THO self-association. The calculated results and the corresponding assignments are illustrated in Table 2. In combination with the analysis in 2D IR correlation spectroscopy, we get to know that free COOH groups will decrease and a cyclic hydrogen-bonded structure may be preferentially formed when THO is added in the imprinting process.

Selective Recognition of THO-Imprinted Polymers. As discussed above, the results of DFT calculation and 2D IR correlation analysis confirm that THO can interact with AA preferentially in the form of a stable cyclic hydrogen-bonded structure which may be the main interaction mode existing in the imprinting process. Herein, methyl acrylic acid (MAA), which is a structural analogue of AA, is used as a functional monomer for comparison.

A similar configuration (complex THO_MAA1) was optimized by the same method, and the results are illustrated in Table 1 and Figure 5a. It is found that MAA can also form a stable cyclic structure with THO. The binding energy of the complex THO_MAA1 (-16.66 kcal mol^{-1}) is close to that of the complex THO_AA1 (-16.63 kcal mol^{-1}), which indicates that MAA is an alternative functional monomer for the preparation of THO-imprinted polymer from the view of binding energy. Furthermore, hydrophobic interaction may also devote to the interaction in the imprinting process due to the presence of the methyl group.[49] As a result, the selectivity of THO-imprinted imprinted polymer with MAA as the functional monomer is slightly higher than that with AA, as confirmed experimentally[25,50] and theoretically[25] in the literatures.

Caffeine (CAF) is a compound that has a methyl group instead of a H group on the 9-nitrogen atom in THO. It is commonly used as an analogue to study the selectivity of THO-imprinted polymer.[12,14] The optimized conformations and binding energies of complexes of CAF-AA are shown in Figure 5 and Table 3, respectively. In comparison with THO, the binding energy of the complex CAF_AA1 (-8.51 kcal mol^{-1}) is obviously lower than that of the complex THO_AA1, which is only equivalent to a single hydrogen-bonded energy. However, the binding energies of the complex CAF_AA2 and the complex CAF_AA3 are approximate with that of the corresponding complex. Thus it is believed that the hydrogen interaction between CAF and AA unit is much weaker than that between THO and the AA unit in the absence of cyclic hydrogen-bonded dimer. The weak hydrogen interaction can decrease the nonspecific binding. As a result, the THO-imprinted polymer shows a high selectivity and binding capacity to THO. This conclusion is also supported by experimental evidence,[14,16] and the typical results are collected in Table 4. Furthermore, it can be deduced from the binding energy results that if CAF was selected as the template, the binding capacity of CAF-imprinted polymer to CAF would be certainly much lower than that of the THO-imprinted polymer to THO, as verified by Ye et al.[12]

Conclusion

Concentration-dependent FT-IR spectra were analyzed using 2D IR correlation spectroscopy with the aid of DFT calculation to study the molecular recognition mechanism of the imprinting process. Based on the binding energy, it is found that the cyclic hydrogen-bonded structure (complex THO_AA1) with the highest binding energy (-16.63 kcal mol^{-1}) can be preferentially formed to other possible configurations. In addition, according to the 2D IR spectra and the theoretical calculation frequencies, the IR bands can be clearly assigned. The bands at 1767, 1735, 1723, 1708, and 1673 cm^{-1} can be ascribed to the C═O

stretching vibrations of free COOH groups, residual carbonyl groups in the complex THO_AA2 and complex THO_AA3, the cyclic hydrogen-bonded structure in dimeric form, and the oligomeric COOH groups, respectively. Furthermore, the structural analogues of AA and THO, MAA and CAF, were also studied. It is found that MAA can also form a stable complex (complex THO_MAA1) with THO due to the high binding energy (-16.66 kcal mol^{-1}). On the other hand, because of the lower binding energy (-8.51 kcal mol^{-1}) for the complex CAF_AA1, CAF has a weak interaction with AA. To sum up, this work has provided a new idea to elucidate the molecular recognition mechanism of THO-imprinted polymers on the basis of 2D IR correlation analysis and DFT calculation. It also verified its reliability by the experimental results as summarized.

Acknowledgment. Financial support from the National Natural Science Foundation of China for Distinguished Young Scholars (grant no. 50625309) is gratefully acknowledged.

References and Notes

(1) Wulff, G.; Sarhan, A. *Angew. Chem., Int. Ed.* **1972**, *11*, 341.
(2) Sellergren, B.; Lepistö, M.; Mosbach, K. *J. Am. Chem. Soc.* **1988**, *110*, 5853.
(3) Yoshikawa, M.; Izumi, J.-i.; Kitao, T.; Koya, S.; Sakamoto, S. *J. Membr. Sci.* **1995**, *108*, 171.
(4) Yoshikawa, M.; Izumi, J.-i. *Macromol. Biosci.* **2003**, *3*, 487.
(5) Ulbricht, M. *J. Chromatogr. B* **2004**, *804*, 113.
(6) Caro, E.; Marce, R. M.; Cormack, P. A. G.; Sherrington, D. C.; Borrull, F. *J. Chromatogr. A* **2003**, *995*, 233.
(7) Beltran, A.; Caro, E.; Marce, R. M.; Cormack, P. A. G.; Sherrington, D. C.; Borrull, F. *Anal. Chim. Acta* **2007**, *597*, 6.
(8) Alexander, C.; Davidson, L.; Hayes, W. *Tetrahedron* **2003**, *59*, 2025.
(9) Andersson, L. I. *J. Chromatogr. B* **2000**, *739*, 163.
(10) Piletsky, S. A.; Piletskaya, E. V.; Panasyuk, T. L.; El'skaya, A. V.; Levi, R.; Karube, I.; Wulff, G. *Macromolecules* **1998**, *31*, 2137.
(11) Haupt, K.; Mosbach, K. *Chem. Rev.* **2000**, *100*, 2495.
(12) Ye, L.; Weiss, R.; Mosbach, K. *Macromolecules* **2000**, *33*, 8239.
(13) Kobayashi, T.; Fukaya, T.; Abe, M.; Fujii, N. *Langmuir* **2002**, *18*, 2866.
(14) Wang, H. Y.; Kobayashi, T.; Fujii, N. *Langmuir* **1996**, *12*, 4850.
(15) Hong, J. M.; Anderson, P. E.; Qian, J.; Martin, C. R. *Chem. Mater.* **1998**, *10*, 1029.
(16) Silvestri, D.; Barbani, N.; Cristallini, C.; Giusti, P.; Ciardelli, G. *J. Membr. Sci.* **2006**, *282*, 284.
(17) Vlatakis, G.; Andersson, L. I.; Muller, R.; Mosbach, K. *Nature* **1993**, *361*, 645.
(18) O'Mahony, J.; Molinelli, A.; Nolan, K.; Smyth, M. R.; Mizaikoff, B. *Biosens. Bioelectron.* **2005**, *20*, 1884.
(19) Li, Y.; Yin, X. F.; Chen, F. R.; Yang, H. H.; Zhuang, Z. X.; Wang, X. R. *Macromolecules* **2006**, *39*, 4497.
(20) Duffy, D. J.; Das, K.; Hsu, S. L.; Penelle, J.; Rotello, V. M.; Stidham, H. D. *J. Am. Chem. Soc.* **2002**, *124*, 8290.
(21) Molinelli, A.; Mahony, J.; Nolan, K.; Smyth, M. R.; Jakusch, M.; Mizaikoff, B. *Anal. Chem.* **2005**, *77*, 5196.
(22) Svenson, J.; Andersson, H. S.; Piletsky, S. A.; Nicholls, I. A. *J. Mol. Recognit.* **1998**, *11*, 83.
(23) Lu, Y.; Li, C. X.; Zhang, H. S.; Liu, X. H. *Anal. Chim. Acta* **2003**, *489*, 33.
(24) Li, Z.; Day, M.; Ding, J. F.; Faid, K. *Macromolecules* **2005**, *38*, 2620.
(25) Dong, W. G.; Yan, M.; Zhang, M. L.; Liu, Z.; Li, Y. M. *Anal. Chim. Acta* **2005**, *542*, 186.
(26) Pavel, D.; Lagowski, J. *Polymer* **2005**, *46*, 7528.
(27) Pavel, D.; Lagowski, J. *Polymer* **2005**, *46*, 7543.
(28) DeChancie, J.; Houk, K. N. *J. Am. Chem. Soc.* **2007**, *129*, 5419.
(29) Noda, I. *Bull. Am. Phys. Soc.* **1986**, *31*, 520.
(30) Noda, I. *J. Am. Chem. Soc.* **1989**, *111*, 8116.
(31) Yamaguchi, Y.; Nge, T. T.; Takemura, A.; Hori, N.; Ono, H. *Biomacromolecules* **2005**, *6*, 1941.
(32) Tang, B.; Wu, P.; Siesler, H. W. *J. Phys. Chem. B* **2008**, *112*, 2880.
(33) Che, A.-F.; Huang, X.-J.; Wang, Z.-G.; Xu, Z.-K. *Aust. J. Chem.* **2008**, *61*, 446.
(34) Ling, J.; Fomina, N.; Rasul, G.; Hogen-Esch, T. E. *J. Phys. Chem. B* **2008**, *112*, 10116.
(35) Becke, A. D. *J. Chem. Phys.* **1993**, *98*, 5648.
(36) Frisch, M. J.; Trucks, G. W.; Schlegel, H. B.; Scuseria, G. E.; Robb, M. A.; Cheeseman, J. R.; Montgomery J.A. Jr.; Vreven, T.; Kudin, K. N.; Burant, J. C.; Millam, J. M.; Iyengar, S. S.; Tomasi, J.; Barone, V.; Mennucci, B.; Cossi, M.; Scalmani, G.; Rega, N.; Petersson, G. A.; Nakatsuji, H.; Hada, M.; Ehara, M.; Toyota, K.; Fukuda, R.; Hasegawa, J.; Ishida, M.; Nakajima, T.; Honda, Y.; Kitao, O.; Nakai, H.; Klene, M.; Li, X.; Knox, J. E.; Hratchian, H. P.; Cross, J. B.; Bakken, V.; Adamo, C.; Jaramillo, J.; Gomperts, R.; Stratmann, R. E.; Yazyev, O.; Austin, A. J.; Cammi, R.; Pomelli, C.; Ochterski, J. W.; Ayala, P. Y.; Morokuma, K.; Voth, G. A.; Salvador, P.; Dannenberg, J. J.; Zakrzewski, V. G.; Dapprich, S.; Daniels, A. D.; Strain, M. C.; Farkas, O.; Malick, D. K.; Rabuck, A. D.; Raghavachari, K.; Foresman, J. B.; Ortiz, J. V.; Cui, Q.; Baboul, A. G.; Clifford, S.; Cioslowski, J.; Stefanov, B. B.; Liu, G.; Liashenko, A.; Piskorz, P.; Komaromi, I.; Martin, R. L.; Fox, D. J.; Keith, T.; Al.Laham, M. A.; Peng, C. Y.; Nanayakkara, A.; Challacombe, M.; Gill, P. M. W.; Johnson, B.; Chen, W.; Wong, M. W.; Gonzalez, C.; Pople, J. A. *Gaussian 03*; Gaussian, Inc.: Wallingford, CT, 2004.
(37) Irikura, K. K.; Johnson, R. D.; Kacker, R. N. *J. Phys. Chem. A* **2005**, *109*, 8430.
(38) Noda, I. *Appl. Spectrosc.* **1993**, *47*, 1329.
(39) Czarnecki, M. A.; Maeda, H.; Ozaki, Y.; Suzuki, M.; Iwahashi, M. *J. Phys. Chem. A* **1998**, *102*, 9117.
(40) Ozaki, Y.; Liu, Y. L.; Noda, I. *Macromolecules* **1997**, *30*, 2391.
(41) Wang, Y.; Murayama, K.; Myojo, Y.; Tsenkova, R.; Hayashi, N.; Ozaki, Y. *J. Phys. Chem. B* **1998**, *102*, 6655.
(42) Nakashima, K.; Ren, Y.; Nishioka, T.; Tsubahara, N.; Noda, I.; Ozaki, Y. *J. Phys. Chem. B* **1999**, *103*, 6704.
(43) Ren, Y. Z.; Shimoyama, M.; Ninomiya, T.; Matsukawa, K.; Inoue, H.; Noda, I.; Ozaki, Y. *J. Phys. Chem. B* **1999**, *103*, 6475.
(44) Lu, X. Y.; Weiss, R. A. *Macromolecules* **1995**, *28*, 3022.
(45) Dong, J.; Ozaki, Y.; Nakashima, K. *Macromolecules* **1997**, *30*, 1111.
(46) Wan, L.-S.; Huang, X.-J.; Xu, Z.-K. *J. Phys. Chem. B* **2007**, *111*, 922.
(47) Nishikawa, Y.; Nakano, T.; Noda, I. *Appl. Spectrosc.* **2006**, *60*, 145.
(48) Nishikawa, Y.; Nakano, T.; Noda, I. *Appl. Spectrosc.* **2007**, *61*, 873.
(49) Nicholls, I. A. *J. Mol. Recognit.* **1998**, *11*, 79.
(50) Sergeyeva, T. A.; Matuschewski, H.; Piletsky, S. A.; Bendig, J.; Schedler, U.; Ulbricht, M. *J. Chromatogr. A* **2001**, *907*, 89.
(51) Ye, L.; Cormack, P. A. G.; Mosbach, K. *Anal. Chim. Acta* **2001**, *435*, 187.
(52) Silvestri, D.; Borrelli, C.; Giusti, P.; Cristallini, C.; Ciardelli, G. *Anal. Chim. Acta* **2005**, *542*, 3.
(53) Wang, H. Y.; Kobayashi, T.; Fujii, N. *J. Chem. Technol. Biotechnol.* **1997**, *70*, 355.
(54) Hattori, K.; Hiwatari, M.; Iiyama, C.; Yoshimi, Y.; Kohori, F.; Sakai, K.; Piletsky, S. A. *J. Membr. Sci.* **2004**, *233*, 169.

JP902163S